NASA TECHNICAL MEMORANDUM

NASA TM X-68105

NASA TM X-68105

INSTALLATION CAUSED FLOW DISTORTION AND ITS EFFECT ON NOISE FROM A FAN DESIGNED FOR TURBOFAN ENGINES

by Frederick P. Povinelli and James H. Dittmar
Lewis Research Center
Cleveland, Ohio

TECHNICAL PAPER proposed for presentation at
Seventh Aerodynamics Testing Conference sponsored by the
American Institute of Aeronautics and Astronautics
Palo Alto, California, September 13-15, 1972

INSTALLATION CAUSED FLOW DISTORTION AND ITS EFFECT ON NOISE FROM A FAN DESIGNED FOR TURBOFAN ENGINES

by Frederick P. Povinelli* and James H. Dittmar**

Lewis Research Center
National Aeronautics and Space Administration
Cleveland, Ohio

Abstract

A ground test stand was used to obtain acoustic data on a full-scale prototype fan designed for quiet subsonic-aircraft engines. The fan was installed in three different ways in the test stand. In two of the installations the fan was driven by a shaft in the inlet; in the third installation the fan was driven from the rear. These three installations, and the structures associated with them, resulted in various amounts of inlet flow distortion to the fan. The rear-drive installation had less inlet flow distortion than the two front drive installations.

Differences in blade passage sound pressure levels of more than 10 dB were measured between the rear-drive and front-drive versions, with the rear-drive installation producing less noise. Perceived noise levels were computed and the influence of the distortion on these levels was determined. Since the fan had its highest noise level in the rear quadrant and since the maximum influence of the inlet distortion on the discrete tone was in the front quadrant, maximum sideline perceived noise levels were increased by only 2 PNdB or less by the increased discrete tones.

Some measurements of inlet flow distortion were made and used in a blade-passage noise generation theory to predict the effects of distortion on noise. Good agreement was obtained when the predicted and measured power level differences between the front-drive and rear-drive installations were compared. Possible origins of the inlet flow distortion were identified.

E-7043

Nomenclature

(Values given are those used for distortion calculations.)

a_m	mean radius on fan disc at which forces act (at 57 percent span for torque force, at 61 percent span for thrust force, at 90 percent span for distortion force)
A_R	area ratio (0.25)
B	number of rotor blades (53)
b	blade width, (in.) (cm)
c	speed of sound, (1116.4 ft/sec) (340.3 m/sec)
c_d	drag coefficient, in tangential direction (0.47)
c_t	thrust coefficient (0.49)
d	distance between blades, (in.) (cm)
$\frac{dc_d}{d\tau}, \frac{dc_t}{d\tau}$	rate of change of thrust and drag coefficients with angle of attack (0.628)
F_d	total drag force (28 100 lbf) (124 905 N)
F_t	total thrust force (20 300 lbf) (90 299 N)
$J_x(Y)$	Bessel function of first kind with order x and argument Y
ℓ	summation index on Fourier analysis of distortion
M_D	rotational Mach number at mean radius where distortion force acts (0.858)
M_{ND}	rotational Mach number at mean radius where torque and thrust forces acts (0.709 and 0.727, respectively)
r	radius of observer from center of fan face (100 ft) (30.5 m)
T	one-half of the angular extent of distortion (5^o, 0.0875 radians)
t	time (sec)
V_B	blade velocity in circumferential direction at mean location of distortion (954 ft/sec) (291 m/sec)
$\bar{v}_z$	average velocity defect in axial direction (ft/sec) (m/sec)
α_1	Fourier coefficient in analysis of force on blade for uniform flow, $\sin(b\pi/d)/2(b\pi/d)$ (b/d taken as 1/2, yielded $\alpha_1 = 1/\pi$)
β_ℓ, δ_ℓ	Fourier coefficients of distortion force analysis. (For no distortion, $\beta_0 = \delta_0 = 1$; $\beta_\ell = \delta_\ell = 0$ for $\ell > 0$)
θ	angle measured around fan from inlet to exhaust; inlet = 0, exhaust = π
τ	angle of attack
Ω	angular velocity of fan (3197 rpm @ 90 percent speed)

Introduction

The full-scale component fan test stand at the Lewis Research Center is being used to study the noise generation of fans which incorporate the latest noise minimization design techniques. Fans for application to both conventional takeoff and

*Engine Systems Section.
**Acoustics Section.

landing (CTOL) and short takeoff and landing (STOL) aircraft engines are being evaluated. The test stand and fan design are described in detail in reference 1. Baseline acoustic results on the first fan tested and some suppression techniques and results are discussed in references 2 and 3, respectively.

A problem uncovered in the course of these initial studies was that of inlet flow distortion caused by the structures associated with the fan installation. Based on Morse and Ingard[4] it was believed that the distortion caused a significant increase in the noise generated at the fan blade passage frequency. In an attempt to minimize the inlet flow distortion, the facility was modified and acoustic data were obtained from a fan installed in three different ways. In this report the installation effects on overall noise, on fan blade passage tone, and on perceived noise levels are discussed.

In order to define the magnitude and extent of the flow distortion, some inlet total pressure measurements were made on one of the fan installations. The distortion values were used in the theory of reference 4 to predict the effects of flow distortion on fan noise generation. The predicted effect was compared to that measured between two installations with different amounts of flow distortion.

Apparatus and Procedure

Fan and Test Stand Description

The 6-foot (1.83 m) diameter fan used in this study was suitable for use on CTOL aircraft in the 20 000 lbf (90 000 N) class. The rotor had 53 blades and the stator 112 blades. The design pressure ratio was 1.5 at a rotor tip speed of 1107 ft/sec (337.4 m/sec). A complete description of the fan design is given in reference 1.

A cutaway view of this fan mounted in the first installation is shown in figure 1. The fan is driven by a shaft in the inlet and some of the concrete support structure is shown extending underneath and upstream of the inlet. A photograph of this fan nacelle assembly, installed at the outdoor test site, is shown in figure 2.

Using electric motors inside the building, the fan was driven through a gearbox and through the shaft shown entering the nacelle (fig. 2). The shaft centerline was 19 ft (5.8 m) above an asphalt ground plane. The swept-shaft-support strut closest to the fan inlet was made in a streamlined airfoil shape to minimize inlet flow distortion. The top of the trailing edge of this strut was approximately 11 ft (3.35 m) upstream of the fan rotor. Open-cell polyurethane foam, 6 in (15.2 cm) thick, was mounted on the drive motor building wall and adequately eliminated reflection effects on the noise data above 400 Hz.[1]

Some measurements made with a total pressure probe in the fan inlet[1,2] indicated that a pressure deficient region existed in the bottom center of the inlet. A sizable blade passage tone measured from the fan installed in this short shaft-front drive installation was attributed to flow distortion. Because of the obstructions upstream of the inlet in this configuration, it was decided to modify the test stand to minimize the presence of any structures which could possibly contribute to flow distortion. The modified stand is shown in figure 3.

The fan was now driven from the rear. The fan and nacelle were moved farther from the building and the shaft was lengthened because of possible high exhaust velocity forces on the building wall. There were no obstructions upstream of the inlet. Before taking acoustic data, polyurethane foam pads were mounted on the building wall as in the previous installation. In order for the fan to be driven from the rear in this installation, a new set of rotor blades were cut identical to those used in the short shaft-front drive installation except that they rotated in the opposite direction.

In spite of the lengthened shaft, deflections of the building wall caused by the force of the fan exhaust jet were excessive. Also, as will be shown later, additional broadband noise generated by the exhaust flowing over the shaft and its supports was intolerable. The final fan installation was arrived at by rotating the fan nacelle, used in the long shaft-rear drive installation, 180° as shown in figure 4 and driving the fan through the inlet. The gearbox was used to reverse the direction of shaft rotation. A gap of 10 ft (3.05 m) between two support pedestals shown in figure 4 eliminated the concrete structure (immediately underneath the inlet) which was present in the short-shaft installation.

A composite plan view of the three installations (fig. 5) shows the microphone locations and the relative positions of the fans. Microphones were positioned on poles around the fan in 10° increments at the shaft centerline elevation. In the short-shaft installation microphones from 70° to 160° were on a 100 ft (30.5 m) radius from the rotor center while those from 10° to 60° were at a fixed 15 ft (4.57 m) from the building wall. The fan rotor plane was 47 ft (14.3 m) from the building wall. For the long-shaft rear-drive installation the microphone poles were repositioned so that all of the microphones were on a 100 ft (30.5 m) radius from the rotor center. The rotor was now 121.5 ft (37 m) from the building wall. In the long-shaft front-drive installation the microphones were not relocated; so the center of the microphone arc was no longer in the plane of the rotor but rather in the exhaust flow. Thus the microphones were no longer placed at equal 10° increments or even 100 ft (30.5 m) distances relative to the rotor. In this installation the rotor was 109.8 ft (33.5 m) from the building.

A list of the test conditions for which acoustic data are reported is given in Table I. Corrected fan speeds were used which corresponded to 60 and 90 percent of standard-day cruise design speed. At 60 percent of design speed, aircraft approach power settings were simulated and at 90 percent of design speed takeoff conditions were approximated. Since corrected fan speeds were set, the mechanical speed and thus rotor blade passage frequency varied somewhat as shown. The three symbols shown in the left-hand column of Table I will be used in future figures to identify the various installations.

Acoustic Instrumentation and Data Reduction

Omnidirectional condenser microphones 0.5 in. (1.3 cm) in diameter were used to pick up the fan noise signals which were then recorded on a 14-channel FM magnetic tape recorder. The acoustic data were resolved into 1/3-octave bands from 50 to 20 000 Hz using a four-second averaging time. Sound pressure levels for three samples for each test condition were averaged, corrected to a 100 ft (30.5 m) distance, and converted to standard day conditions (70 percent relative humidity, 59° F (288.2 K)) using the methods of reference 5. No corrections were made for ground reflection effects. The data tapes were also reduced on a 32-Hertz constant bandwidth analyzer from 0 to 10 000 Hz.

Distortion Tests

In order to define the origin, extent, and magnitude of the flow distortion in a front-drive installation, some tests were made using a 1.4 pressure-ratio fan in the long-shaft front-drive installation. The 1.5 pressure-ratio fan in this installation was not instrumented for distortion measurements since the primary objective in testing it was to measure its noise output. The 1.4 pressure-ratio fan was designed to be identical to the 1.5 pressure-ratio fan except that the rotor and stator blades had less camber, thus generating the lower pressure rise for the same weight flow. It was assumed that the installation caused flow distortions were identical for these two similar fans.

Measurements of the distortion were made in the fan inlet using a multi-tube total pressure rake with tubes on 1/2 inch (0.3 cm) centers. The rake covered an area approximately 4 × 6 in. (10.2 × 15.2 cm). Previous distortion measurements[1,2] made on the 1.5 pressure-ratio fan in the short-shaft installation were taken with a much larger rake and showed that the distortion was confined to a small region in the bottom center of the inlet. The tubes in this rake were not spaced closely enough to adequately characterize the distortion, however. Thus the rake used in this study was designed with 88 closely spaced tubes. It was installed in the inlet at the 6 o'clock position and was located approximately 1 ft (0.3 m) upstream of the rotor. Visual observations of the flow field around the inlet were also made by locating yarn tufts on the streamlined drive-shaft strut, on eight horizontal wires strung underneath the inlet, on vertical wires mounted beneath and downstream of the bellmouth, and around the outer casing at the bellmouth-inlet flange.

Results and Discussion

Since the quiet fan test rig is used to evaluate the acoustic performance of component fans, inlet flow distortion instrumentation is not installed as a matter of practice. Thus distortion measurements were not made for each installation considered herein. It is reasonable to assume, however, that different amounts of inlet flow distortion existed for each installation even though no comparative inlet pressure measurements are available. The rear-drive installation presented no obstructions upstream of the inlet and should therefore have the least inlet flow distortion of the configurations tested.

As noted earlier, some distortion measurements were made for a 1.4 pressure-ratio fan installed in the long-shaft front-drive configuration. For this installation the distortion was characterized well enough to allow a calculation to be made to predict the effects of this distortion on the fan noise. The distortion results will be discussed after noise data comparisons are made for the three installations.

Noise Comparisons

Overall sound pressure levels (OASPL) for the three installations are shown in figure 6 as a function of angular position from the inlet. The two front drive installations have about the same overall levels for both speeds except at angles greater than about 130° and at two angles in the front quadrant at nominally 20° and 50°. Although a calibration error is suspected at these two front quadrant angles these readings have been reported as measured since they do not significantly affect the results. Aft of 130° the difference in OASPL between the two front-drive installations are essentially unexplained but may have been due to a change in the exhaust nozzle which changed the nozzle contraction and the exposed length of tail cone (compare figs. 2 and 4). A feature to note in figure 6 is the generally higher OASPL values for the rear-drive installation in comparison to the two front drive versions. Low frequency noise controlled the rear-drive OASPL (as will be shown) especially for the rear quadrant angles.

Comparisons of narrow-band spectra for the three installations are given in figure 7 for 90 percent speed. Figure 7(a) is for a nominal angular position of approximately 50° where the front-quadrant noise peaked, and figure 7(b) is for the approximate rear-quadrant noise peak at 120°. The large peaks in the spectra at 2850 to 2950 Hz correspond to the blade-passage frequency while the smaller peaks are at harmonics of the fundamental frequency. In the front quadrant, the blade-passage tone and its harmonics were substantially lower for the rear-drive installation than for the two front-drive cases because of the lower inlet flow distortion for the rear-drive installation. Higher low-frequency noise for the rear-drive case is evident below about 2100 Hz. This was caused by the noise generated from the high velocity fan exhaust flow impinging and scrubbing on the drive shaft, its supports, and the concrete structures. Over the rest of the spectrum the broadband noise of the three installations was comparable. The blade-passage tone in the aft quadrant (fig. 7(b)) for the rear-drive installation was still less than for the front drive cases but not as markedly as in the front quadrant. Comparison of the broadband levels in figure 7(b) shows the rear-drive level higher over the entire spectrum. This broadband level is higher at 120° than at 50° because of the proximity of the measurement to the exhaust-flow-generated noise. Thus, in addition to the building wall deflections caused by the exhaust jet force in the rear-drive installation, high-level broadband noise also made this installation unacceptable.

Since the discrete tones most dramatically manifest the effects of the type of inlet flow distortion present in this rig, blade-passage tones have been determined from the narrow-band

spectra and are shown in figure 8 for all angles. All values given are the acoustic energy average of the blade-passage tones measured from at least three separate samples at each angle. For 90 percent speed (fig. 8(a)) the rear-drive installation with the least flow distortion had consistently lower levels than did the two front-drive installations with higher levels of inlet flow distortion. The largest differences occurred in the forward radiated noise with a maximum difference of at least 10 dB over the front 70° when comparing the rear-drive version to the short shaft-front drive version. A somewhat lesser blade-passage tone was generated in the front quadrant when the front-drive installation was run with the long shaft as compared to the short shaft. At 60 percent speed (fig. 8(b)) the rear-drive installation still had consistently less blade-passage tone content but not nearly as great a difference as at the higher speed.

One-third octave spectra for the same angles as shown for the narrow band spectra (fig. 7) are presented in figure 9. For both angles the two front-drive installations have very similar sound pressure levels. The rear-drive installation had higher levels up to the 2500 Hz band in the front quadrant (fig. 9(a)) and over the entire spectrum in the aft quadrant (fig. 9(b)).

To determine the effect of flow distortion on subjective perceived noise levels, it was reasoned that elimination of the flow distortion would result in the front-drive installations having discrete tones at least as low as those measured for the cleaner-flow rear-drive installation. The method of correcting the 1/3-octave spectra is illustrated by use of figure 10. Blade passage tones measured from the rear-drive narrow-band spectra were added to the faired-in broadband levels from the front-drive spectra to obtain the corrected spectra. Since the blade-passage tone was split between two one-third octave bands it was necessary to correspondingly split the rear-drive blade-passage tone before addition to the broadband level.

Correcting the one-third octave spectra in this way influenced sideline perceived noise levels as shown in figure 11 for 90 percent speed. Perceived noise levels were calculated according to the methods described in reference 6. A sideline distance of 1000 ft (305 m) was chosen as representative of the altitude of an airplane at the FAA takeoff noise certification point. Differences as great as 6 PNdB in the front quadrant are evident in figure 11 when the discrete tone corrections are made. As expected from the blade-passage tone comparisons (fig. 8), smaller differences resulted in the aft quadrant.

One noise rating for a fan or engine is its maximum sideline PNdB. Since the fan tested in this study had its maximum PNdB level occur in the aft quadrant where the distortion had less affect on the blade-passage tone, the maximum PNdB rating was only affected by about 2 PNdB. If a subsonic tip speed fan were tested whose maximum level occurred in the front quadrant and was substantially above the aft quadrant levels, significantly higher maximum PNdB levels than for a clean inlet configuration could result. Although not shown here, at approach conditions of 60 percent speed and 370 ft (113 m) sideline distance the corrections for discrete tones resulted in only a 2 PNdB, or less, reduction over the entire angular range.

Distortion Results and Analysis

The total pressure measurements made in the inlet of the long-shaft front-drive installation showed that the distortion was confined to a small area approximately 4 × 6 in. (10.2 × 15.2 cm) in the bottom center of the inlet. The distortion fluctuated in amplitude and shifted slightly in circumferential location but generally was contained within the measuring rake. Observation of the tufts showed that the distortion most likely originated either from flow over the concrete support structure still present upstream of the inlet or from the fan nacelle support underneath and behind the inlet. Flow was being pulled into the inlet from downstream as evidenced by the direction of the tufts placed around the bellmouth-inlet flange.

The inlet pressure measurements were converted to velocities and used in the propeller sound generation theory of Morse and Ingard[4] to calculate the additional sound power generation in a nonuniform flow field. In the interest of simplicity, some assumptions were made in the application of this theory to a ducted fan. Other work[7,8] points out the importance of considering duct modes. Duct cutoff theory predicts that the noise from the inlet flow distortion would propagate out of the inlet because the modes generated by the interaction of the single cell of distortion and the rotor blades are not cutoff. The uniform flow noise levels, on the other hand, would be cut off according to the theory. However, in reference 9 it has been shown that cutoff apparently only accounts for a 3 to 5 dB noise reduction as opposed to much larger predicted reductions. This is possibly due to free stream turbulence levels, for instance, which could modify the cutoff theory. Thus as a first approximation, duct mode effects were not included here but rather only the simpler free-propeller theory was used to predict the effects of distortion on noise in this outdoor full-scale fan rig. Further work may indeed show that consideration of the duct effects could improve the agreement between prediction and measurement already obtained in this report. Since it is also recognized that the directivity of the sound is probably affected by the presence of the duct, only power levels in the front quadrant were compared between the long-shaft front-drive and rear-drive installations.

Considering only the blade-passage tone propagating at the same elevation as the fan centerline, the equation for the sound pressure from reference 4 (Eq. (11.3.20)) becomes

$$p = \frac{B\Omega\alpha_1}{2c\pi r}\left\{\sum_{\ell=0}^{\infty}\left(\delta_\ell \frac{B-\ell}{BM} F_d - \beta_\ell F_t \cos\theta\right)J_{B-\ell}\right.$$

$$(BM \sin\theta)\sin\left[\frac{B\Omega}{C}(r - ct) + (B-\ell)\frac{\pi}{2}\right]$$

$$\left. + \sum_{\ell=0}^{\infty}\left(\delta_\ell \frac{B+\ell}{BM} F_d - \beta_\ell F_t \cos\theta\right)J_{B+\ell}\right.$$

$$\left.(BM \sin\theta)\sin\left[\frac{B\Omega}{C}(r - ct) + (B+\ell)\frac{\pi}{2}\right]\right\} \quad (1)$$

These coefficients apply only over a small radial extent (fig. 12) and thus must be proportioned by the ratio, A_R, of the shaded region to the entire sector.

After substitution of Equations (2) to (5) in Equation (1), the summations in Equation (1) were first divided into the $\ell = 0$ terms and the $\ell > 0$ terms. Then the $\ell = 0$ part was further broken up into that part which is the no distortion part and that which arises from the distortion. The resulting equation is:

$$p = \frac{B\Omega\alpha_1}{2\pi cr}\left\{\left[2\left(\frac{F_d}{M_{ND}} - F_t\cos\theta\right)J_B(BM_{ND}\sin\theta)\sin\left[\frac{B\Omega}{c}(r-ct) + \frac{B\pi}{2}\right]\right]\right.$$

($\ell = 0$ no distortion part)

$$+ A_R\left[2\left(\left(\frac{1}{\pi c_d}\frac{dc_d}{d\tau}\frac{\bar{v}_z}{V_B}TF_d}{M_D} - \frac{1}{\pi c_t}\frac{dc_t}{d\tau}\frac{\bar{v}_z}{V_B}TF_t\cos\theta\right)J_B(BM_D\sin\theta)\sin\left[\frac{B\Omega}{c}(r-ct) + \frac{B\pi}{2}\right]\right]\right.$$

($\ell = 0$ distortion part)

$$+ A_R\left[\sum_{\ell=1}^{\infty}\left(\frac{(B-\ell)F_d}{BM_D\ell\pi c_d}\frac{dc_d}{d\tau}\frac{\bar{v}_z}{V_B}\sin(\ell T) - \frac{F_t\cos\theta}{\ell\pi c_t}\frac{dc_t}{d\tau}\frac{\bar{v}_z}{V_B}\sin(\ell T)\right)J_{B-\ell}(BM_D\sin\theta)\right.$$

$$\times \sin\left[\frac{B\Omega}{c}(r-ct) + (B-\ell)\frac{\pi}{2}\right]$$

$$\left.\left. + \sum_{\ell=1}^{\infty}\left(\frac{(B+\ell)F_d}{BM_D\ell\pi c_d}\frac{dc_d}{d\tau}\frac{\bar{v}_z}{V_B}\sin(\ell T) - \frac{F_t\cos\theta}{\ell\pi c_t}\frac{dc_t}{d\tau}\frac{\bar{v}_z}{V_B}\sin(\ell T)J_{B+\ell}(BM_D\sin\theta)\sin\left[\frac{B\Omega}{c}(r-ct) + (B+\ell)\frac{\pi}{2}\right]\right]\right\}$$

($\ell > 0$ distortion terms)

(6)

Following reference 4 the evaluation of the coefficients β and δ was accomplished by assuming an airfoil with a constant linear lift curve slope and determining the change in lift and drag forces resulting from an incoming velocity defect. This lift curve slope is assumed not to be influenced by the frequency at which the velocity defect is seen by the blade. The defect occurred over a small part of the fan disc and to simplify the calculations an average velocity defect, $\bar{v}_z$, was taken as shown in figure 12. From Fourier analysis of this defect around the inlet, the coefficients resolve as

$$\beta_0 = 1 + \frac{1}{\pi c_t}\frac{dc_t}{d\tau}\frac{\bar{v}_z}{V_B}T \quad (2)$$

$$\delta_0 = 1 + \frac{1}{\pi c_d}\frac{dc_d}{d\tau}\frac{\bar{v}_z}{V_B}T \quad (3)$$

$\ell = 0$

$$\beta_\ell = \frac{1}{\ell\pi c_t}\frac{dc_t}{d\tau}\frac{\bar{v}_z}{V_B}\sin(\ell T) \quad (4)$$

$$\delta_\ell = \frac{1}{\ell\pi c_d}\frac{dc_d}{d\tau}\frac{\bar{v}_z}{V_B}\sin(\ell T) \quad (5)$$

$\ell > 0$

Values of the aerodynamic parameters were determined from detailed blade element data obtained on a 1/4-scale model of the fan.

The RMS sound pressure was calculated from equation 6 for both the uniform flow and the distortion cases at each front quadrant angle. Sound pressure levels and subsequently front quadrant sound power levels (PWL) were computed. Differences between the distortion and uniform flow PWL for blade passage tone at 90 percent speed are shown as a function of distortion in figure 13. The two curves are for the blade forces applied at 57 and 61 percent of blade span. From the scale model testing the torque force was applied at 57 percent of blade span and the thrust force at 61 percent span. The resultant mean force location would be somewhere between these two limits. Since the amplitude of the distortion fluctuated somewhat, a number of averages of the distortion were taken when the disturbance was fully contained in the rake. The fluctuation of this average is represented by the range on $\bar{v}_z/V_B$ shown in figure 13. The measured power level difference between the long-shaft front drive and the rear drive installations is shown as the dashed horizontal line.

The calculation slightly overpredicted the noise increase caused by the inlet flow distortion. One possible explanation is that in the rear-drive installation some distortion may still exist due to the unstreamlined structure underneath and downstream of the inlet. The experimentally determined PWL differences would then be lower than would be measured if the rear-drive case had perfectly uniform inlet flow. Another possible reason for the overprediction stems from the fact that the calculated force fluctuations on the rotor blades caused by the inlet flow distortion may be too high. The method used by Morse and Ingard assumed that the lift curve slope was not influenced by the frequency at which the blades experienced the velocity defect. Because it is likely that the blades do not respond instantaneously to a change in angle of attack as they go through the distortion[10,11] they may not exhibit the total lift fluctuation as assumed in the method of calculated used here. This would result in lower values for β and δ and consequently somewhat less noise would be predicted in the distortion case. A more detailed discussion of the theory and its application is given in reference 12.

Summary of Results

1. A fan was installed in three different ways in an outdoor noise test stand. In two of the installations the fan was driven by a shaft in the inlet whereas in the other installation the fan was driven from the rear. The two front-drive installations had more inlet flow distortion than the rear-drive case due to structures in the flow path upstream of the inlet. Differences of more than 10 dB in blade-passage tone were observed between the rear-drive and front-drive versions, with the rear drive installation producing less blade-passage noise. Differences were the greatest in the front quadrant.

2. In spite of the greatly reduced blade-passage tone, the rear-drive installation was unacceptable from a noise standpoint because of the high dB level, low frequency noise generated by exhaust flow over supporting structures.

3. Noise spectra of the front-drive installations were corrected to have discrete tones of the magnitude measured for the cleaner inlet rear-drive installation. Maximum sideline perceived noise levels were reduced less than about 2 PNdB when corrected because the fan was aft-quadrant dominant and the maximum influence of distortion occurred in front of the fan.

4. Inlet flow distortion measurements were made for a fan installed in the long-shaft front-drive installation. These measurements were used in a blade-passage noise generation theory to predict the effects of distortion on noise. Good agreement was obtained between the predicted effect and the noise difference measured between the front-drive and rear-drive installations.

References

1. Leonard, B. R., Schmiedlin, R. G., Stakolich, E. G., and Neumann, H. E., "Acoustic and Aerodynamic Performance of a 6-Foot-Diameter Fan for Turbofan Engines. I - Design of Facility and QF-1 Fan," TN D-5877, 1970, NASA, Cleveland, Ohio.

2. Goldstein, A. W., Lucas, J. G., and Balombin, J. R., "Acoustic and Aerodynamic Performance of a 6-Foot-Diameter Fan for Turbofan Engines. II - Performance of QF-1 Fan in Nacelle Without Acoustic Suppression," TN D-6080, 1970, NASA, Cleveland, Ohio.

3. Rice, E. J., Feiler, C. E., and Acker, L. W., "Acoustic and Aerodynamic Performance of a 6-Foot-Diameter Fan for Turbofan Engines. III - Performance With Noise Suppressors," TN D-6178, 1971, NASA, Cleveland, Ohio.

4. Morse, P. M., and Ingard, K. U., Theoretical Acoustics, McGraw-Hill, New York, pp. 737-750, 1968.

5. Anon., "Standard Values of Atmospheric Absorption as a Function of Temperature and Humidity for Use in Evaluating Aircraft Flyover Noise," Aerospace Recommended Practice 866, 1964, SAE, New York, N.Y.

6. Anon., "Definitions and Procedures for Computing the Perceived Noise Level of Aircraft Noise," Aerospace Recommended Procedure 865A, Aug. 1969, SAE, New York, N.Y.

7. Tyler, J. M. and Sofrin, T. G., "Axial Flow Compressor Noise Studies." SAE Transactions, Vol. 70, 1962, pp. 309-332.

8. Hubbard, H. H., Lansing, D. L., and Runyan, H. L., "A Review of Rotating Blade Noise Technology," Symposium on Aerodynamic Noise, Loughborough Univ. of Technology, 1970, pp. D.I.I-D.1.43.

9. Kramer, J. J., Sofrin, T. G., Klapproth, J. F., Leonard, B. R., and Hartmann, M. J., "Fan Noise and Performance," Aircraft Engine Noise Reduction Conference, Lewis Research Center, May 16-17, 1972. NASA Special Publication, to be published.

10. Sears, W. R., "Some Aspects of Non-Stationary Airfoil Theory and Its Practical Application." Journal of the Aeronautical Sciences, Vol. 8, No. 3, Jan. 1941, pp. 104-108.

11. Kemp, N. H. and Sears, W. R., "The Unsteady Forces Due to Viscous Wakes in Turbomachines." Journal of the Aeronautical Sciences, Vol. 22, no. 7, July 1955, pp. 478-483.

12. Povinelli, F. P., Dittmar, J. H., and Woodward, R. P., "Effects of Installation Caused Flow Distortion on Noise From a Fan Designed for Turbofan Engines," proposed Technical Note, 1972, NASA, Cleveland, Ohio.

TABLE I. - ACOUSTIC TEST CONDITIONS

Installation	Temperature, °F (K)	Relative humidity, percent	Wind velocity, knots (km/hr)	Percent of design speed (sea level corrected)	Mechanical rotor speed, rpm	Blade-passage frequency, Hertz
Short shaft-front drive 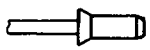	28 (271)	72	6-10 (11.1-18.5)	60	2057	1921
				90	3084	2724
Long shaft-rear drive 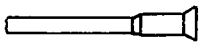	26 (270)	78	3-6 (5.6-11.1)	60	2045	1910
				90	3064	2708
Long shaft-front drive 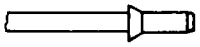	55 (286)	78	5 (9.3)	60	2112	1971
				90	3167	2798

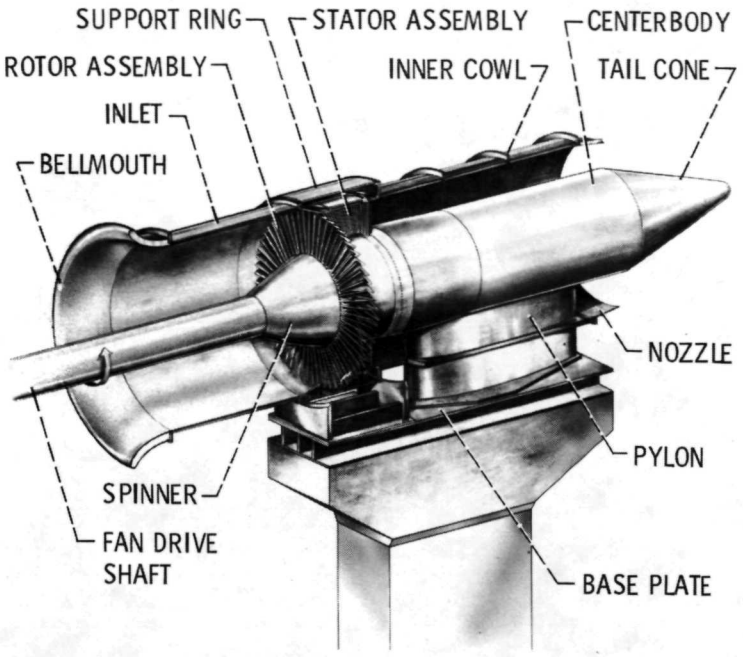

Figure 1. - Front-drive fan nacelle assembly.

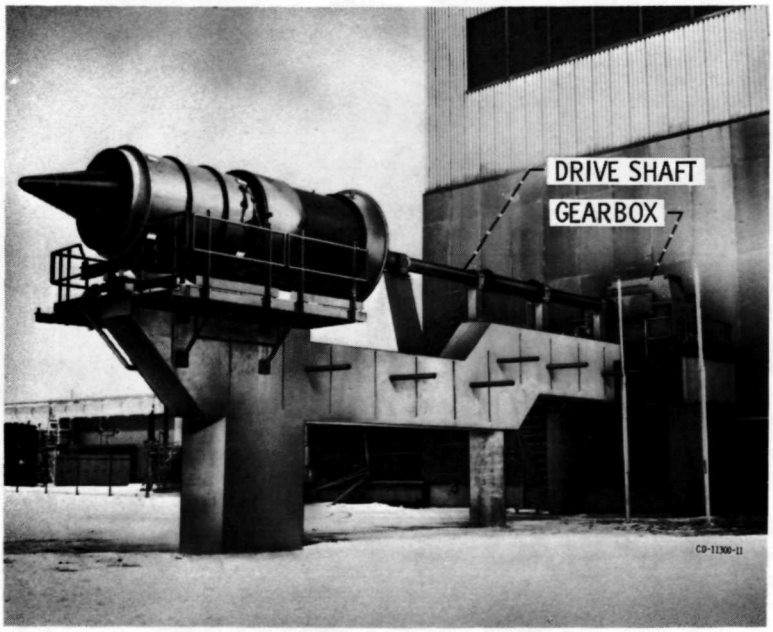

Figure 2. - Short shaft-front drive installation.

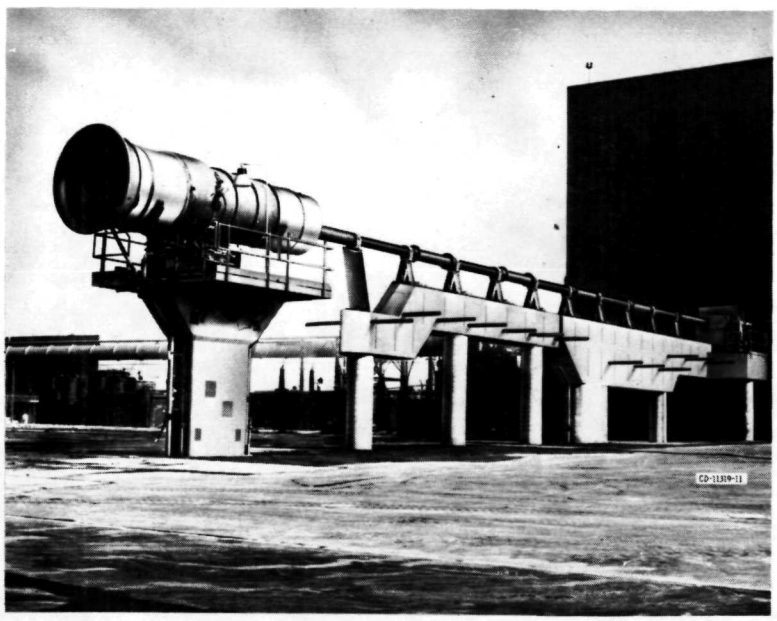

Figure 3. - Long shaft-rear drive installation.

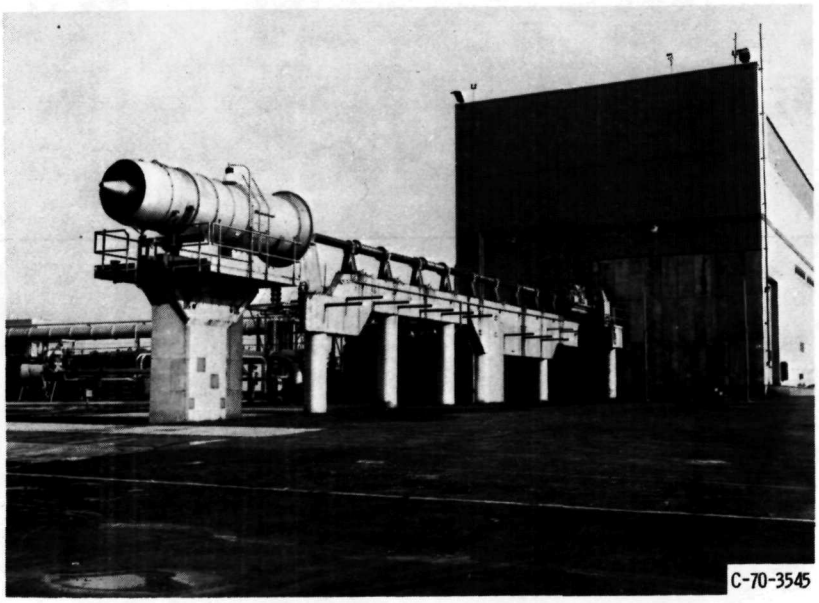

Figure 4. - Long shaft - front drive installation.

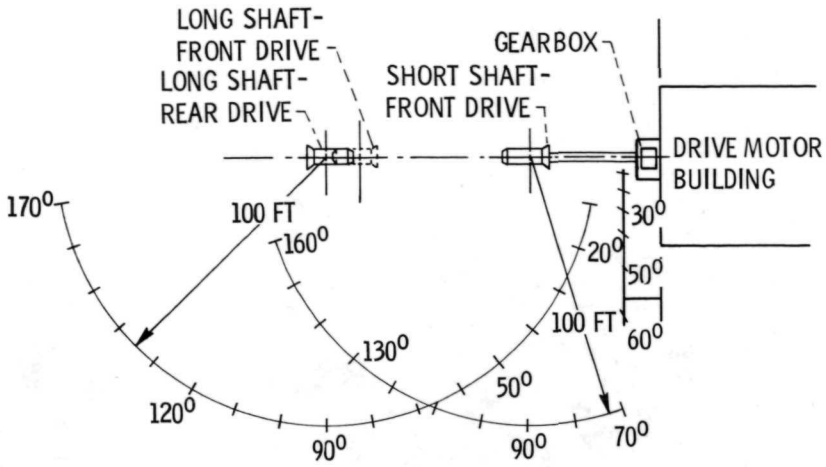

Figure 5. - Plan view of fan installations.

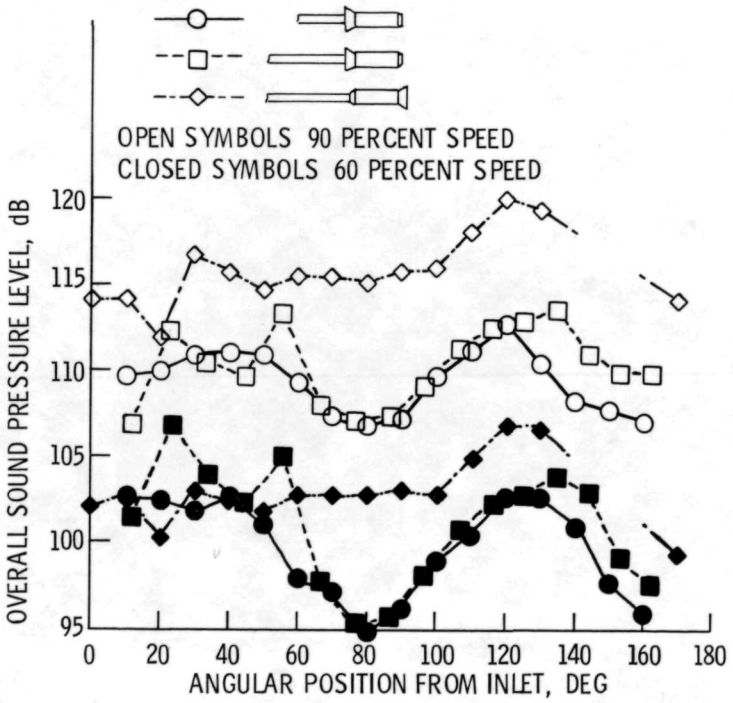

Figure 6. - Angular distribution of overall sound pressure level on 100 foot (30.5 m) radius for three fan installations. (Standard-day conditions.)

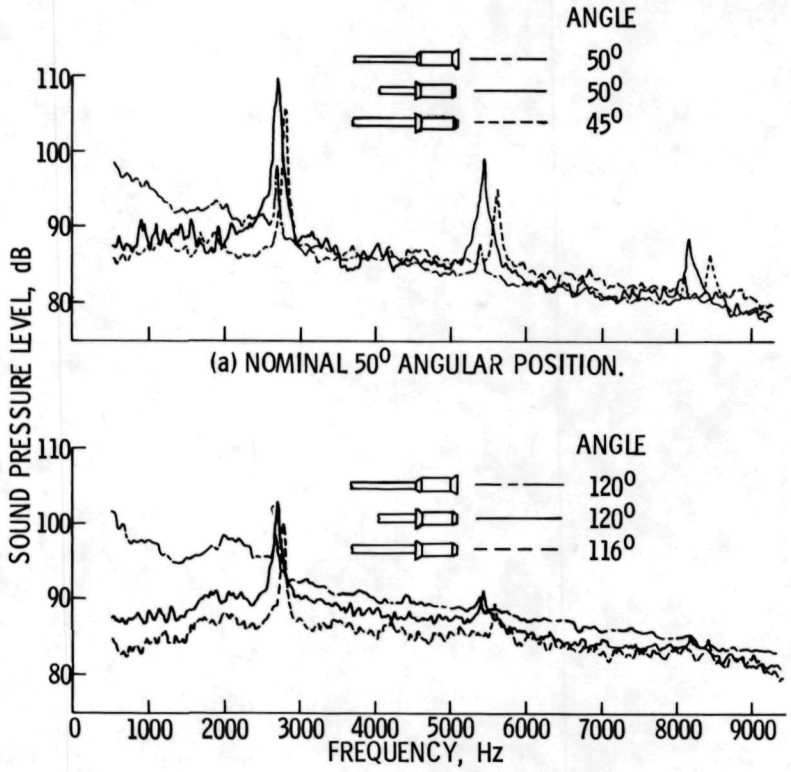

(a) NOMINAL 50° ANGULAR POSITION.

(b) NOMINAL 120° ANGULAR POSITION.

Figure 7. - Narrow-band (32 Hz bandwidth) sound pressure level spectra on a 100 foot (30.5 M) radius; 90 percent speed.

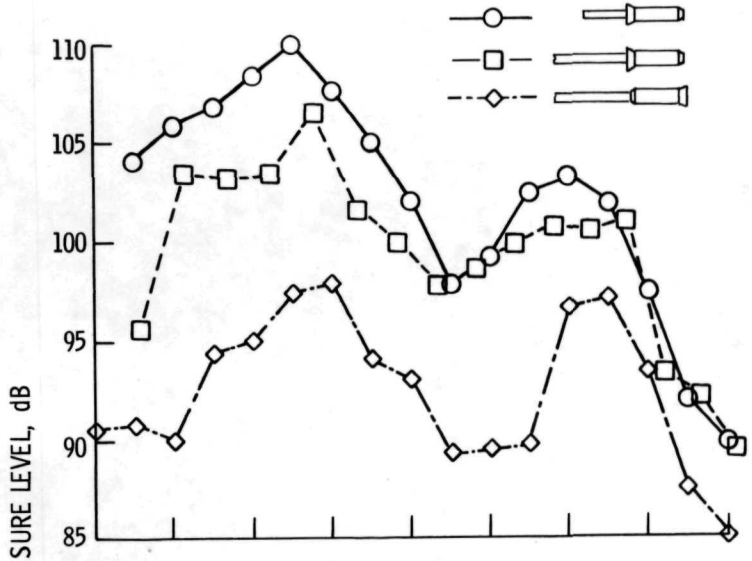

(a) 90 PERCENT SPEED.

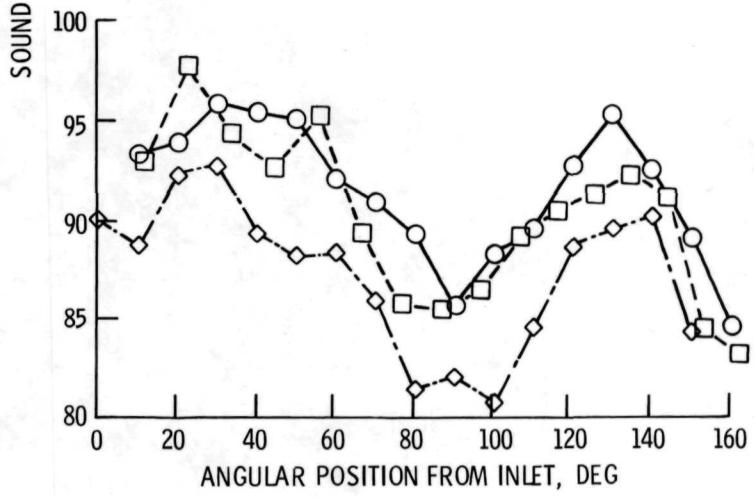

(b) 60 PERCENT SPEED.

Figure 8. - Angular distribution of blade-passage tone from narrow band spectra at standard-day conditions on a 100 foot (30.5 m) radius.

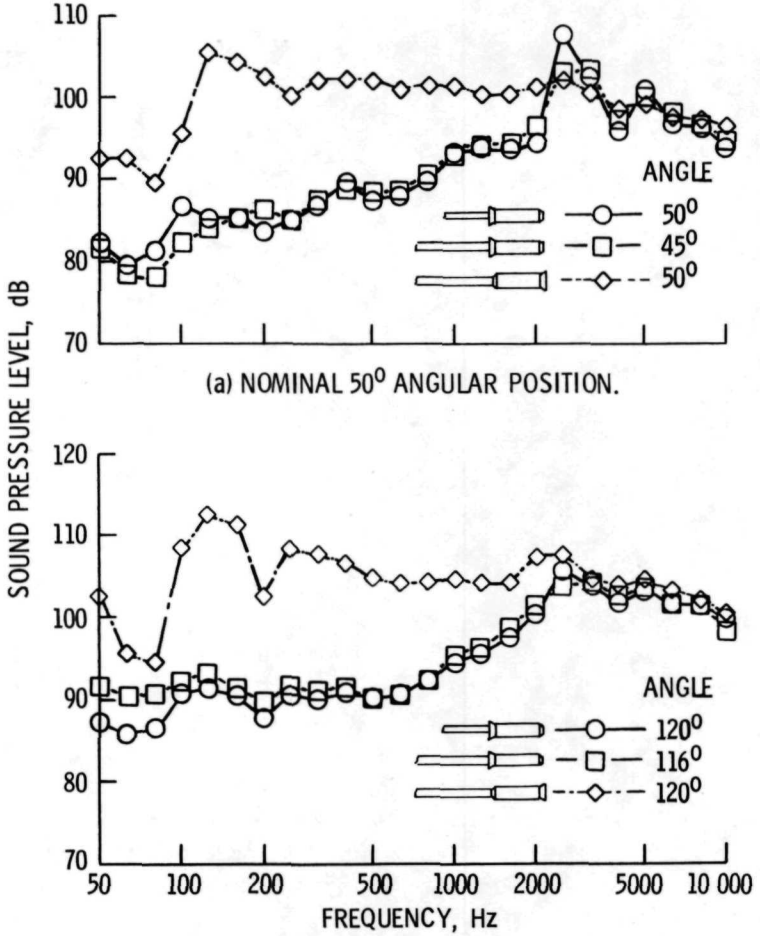

(a) NOMINAL 50° ANGULAR POSITION.

(b) NOMINAL 120° ANGULAR POSITION.

Figure 9. - One-third octave sound pressure level spectra on a 100 foot (30.5 m) radius; 90 percent speed. (Standard-day conditions.)

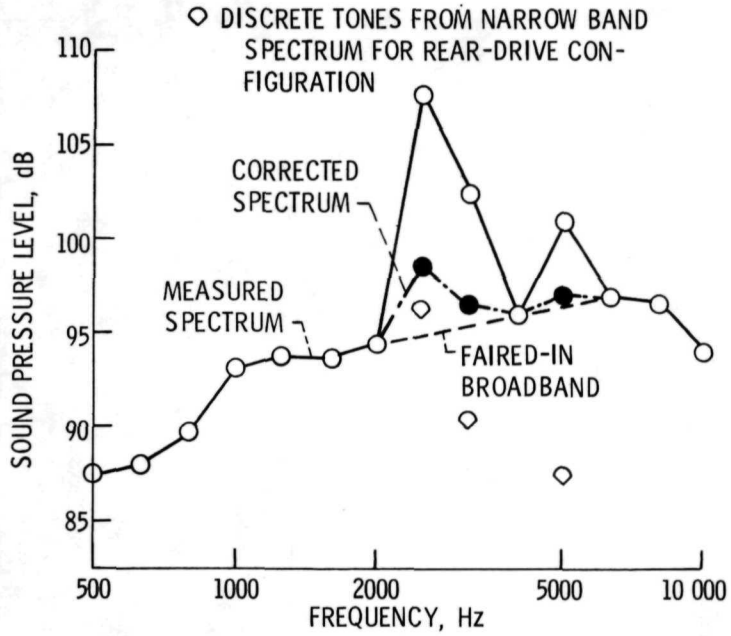

Figure 10. - Method of correcting one-third octave spectra for blade-passage tone; short shaft-front drive configuration, 50° angular position, 90 percent speed.

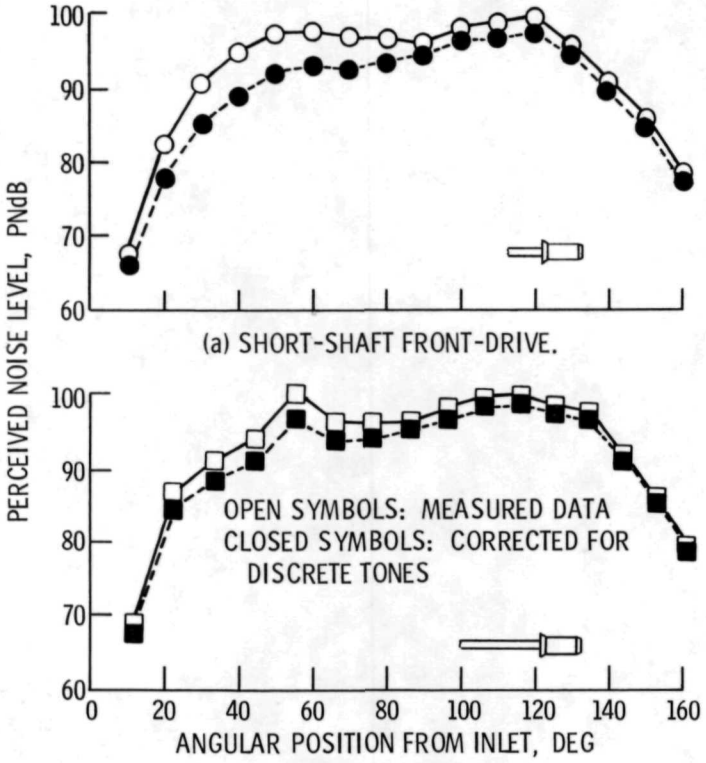

Figure 11. - Comparison of measured sideline perceived noise levels with discrete tone corrected perceived noise levels; 90 percent speed, 1000 foot (305 m) sideline.

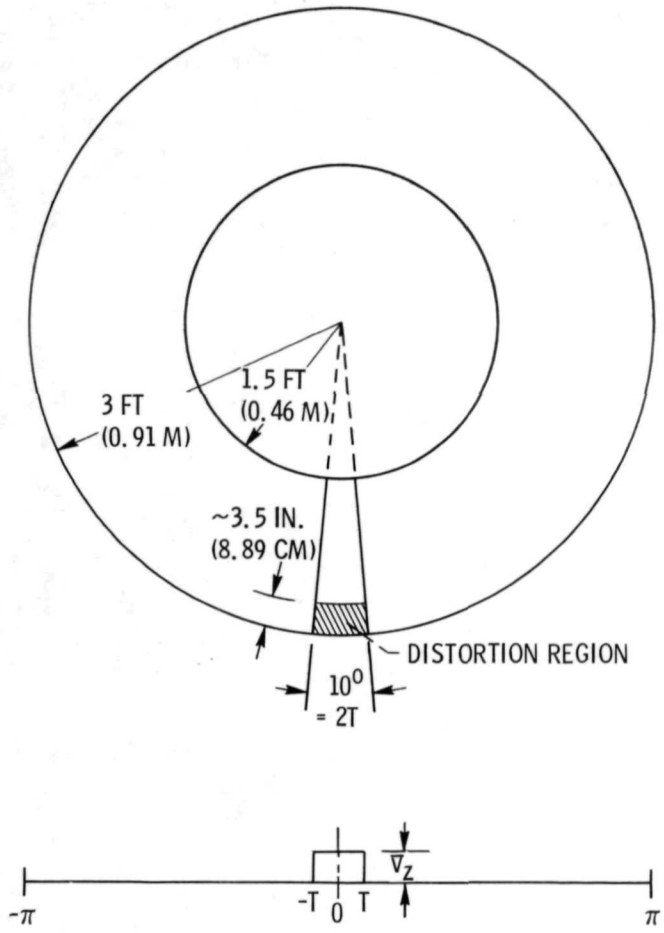

Figure 12. - Extent and characterization of distortion.

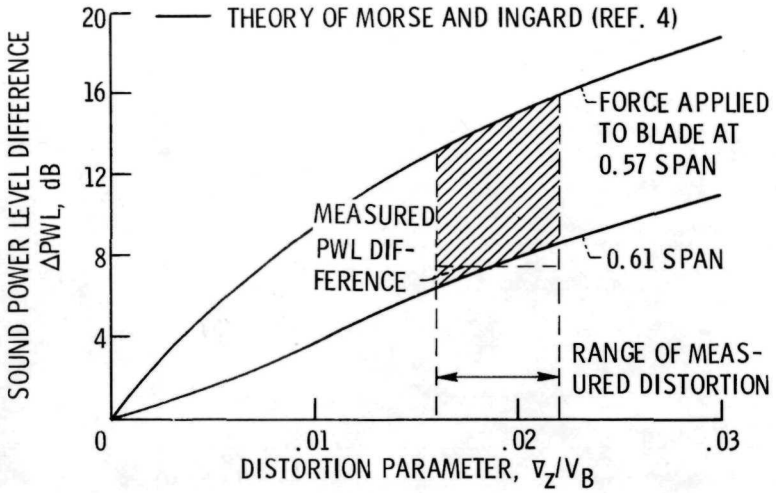

Figure 13. - Sound power level difference for front 90°, 90 percent speed.